ISSN: 2277-9655
Impact Factor: 4.116
CODEN: IJESS7

IJESRT

INTERNATIONAL JOURNAL OF ENGINEERING SCIENCES & RESEARCH TECHNOLOGY

AERODYNAMICS AND STATIC STABILITY INVESTIGATION OF A V-TAIL LAYOUT USING CFD METHODS AND VARIOUS TURBULENCE MODELS

Georgios N. Kollias*, Michail T. Koufopoulos, D.E. Mazarakos, D-E. Margaris, V.Kostopoulos
* Department of Mechanical Engineering and Aeronautics, University of Patras, 26500 Patras, Greece

DOI: 10.5281/zenodo.225382

ABSTRACT

In this paper, the conversion of a T-tail aircraft model to Vee-tail has investigated. Analytical research was carried out for the geometry of the tail as well as for the selection of the airfoil of the model, which specifically is NACA 64A010. Moreover, a 2-D computational analysis was set, for the airfoil investigation at Reynolds 130.000 and a 3-D computational analysis was performed for the Vee-tail for different angles of attack and side-slip, using the turbulent models Spalart-Allmaras, Realizable k-ε and SST k-ω.

The analysis concludes that the experimental, theoretical and analytical results are in agreement with the computational process. For the Vee-tail, the analysis shows that the C_L follows a linear variation in relation with the angle of attack up to 7° whereas the results with the turbulent models begin to deviate. In addition, for the C_D relative to the angle of attack, a convergence among the various turbulent models as well as with the theoretical results was observed.

With the increase of the sideslip angle, loss of the aerodynamic performance of the Vee-tail model is observed. At 8°, the C_D increases 30% while the C_L decreases 9%. For the 12°, the C_D increases dramatically up to 76% and at 24°, the aerodynamic performance is completely reduced to zero.

KEYWORDS: Vee-tail, V-tail, Aerodynamics, CFD, Turbulence Models, Sideslip

INTRODUCTION

Computational Fluid Dynamics (CFD) is a new numerical tool used for the prediction of the flow field around bodies. It is based on the finite volume method and the Navier-Stokes equations. The objective of this work is the conversion of the T-tail unmanned air-vehicle ATLAS I to Vee-tail and the computational analysis using the CFD in order to estimate the flow distribution around the Vee-tail empennage structure. An extensive survey was carried out on the geometrical characteristics of the tail, as well as the selection of the Vee-tail airfoil for ATLAS I which is NACA 64A010 [12]. A 2-D computational analysis on the airfoil at the cruising speed of the aircraft (12m/s) and Reynolds number 128.976 was set. Verifying the 2-D computational model using experimental data, the mesh quality and density was selected for 3-D analysis. A 3-D computational analysis was set for the Vee-tail in various angles of attack and sideslip with the turbulent models Spalart-Allmaras, Realizable k-ε and SST k-ω, in order to calculate the aerodynamic coefficients. The lack of wind tunnel testing led the investigation to use different turbulent models for the simulation. The analysis starts with a study of the T-tail section of ATLAS I aircraft which was designed and manufactured at the University of Patras. The new Vee-tail has to reach the same stability characteristics with the T-tail configuration in order to avoid any malfunctions in the flying performance of the aircraft. The geometrical and aerodynamical characteristics of the aircraft are presented in Table 1 [7].

ISSN: 2277-9655
Impact Factor: 4.116
CODEN: IJESS7

Table 1: Geometrical and Aerodynamic Characteristics of ATLAS I.

ATLAS I AIRCRAFT									
T-TAIL GEOMETRY				FLIGHT PARAMETRES			WING GEOMETRY		
V_h	0.4		Λ_v	40.43°	U (m/s)	12		Sw (m2)	0.45504
V_v	0.032		$(c_{tip})_h$ (m)	0.126	OPERATING ALTITUDE (m)	60		bw (m)	1.58
X_h (m)	0.662		$(c_{root})_h$ (m)	0.126				cw (m)	0.288
X_v (m)	0.61		$(c_{tip})_v$ (m)	0.100	T-TAIL AERODYNAMICS - AIRFOILS				
AR_h	5		$(c_{root})_v$ (m)	0.244	HORIZONTAL STABILIZER NACA0012 @ 106000 Reynolds		$(C_{l_a})_h$	0.1164 deg^{-1}	
AR_v	1.8		b_h (m)	0.632					
I_h	-5°		b_v (m)	0.222					
I_v	5°		λ_h	1	VERTICAL STABILIZER NACA0015 @ 154000 Reynolds		$(C_{l_a})_v$	0.13 deg^{-1}	
Λ_h	0°		λ_v	0.4					
$S_v(m^2)$	0.038		$S_h(m^2)$	0.08					

Fig 1: ATLAS I Aircraft.

For each section of the tail the C_{l_a} of airfoil was transformed to C_{L_a} for finite wing using the formulas:

$AR \geq 4$ $\quad (C_{L_a})_h = \frac{(Cla)_h}{1+(Cla)_h/(\pi AR_h)}$ (1) [13]

$AR < 4$ $\quad (C_{L_a})_v = \frac{(Cla)_v}{\sqrt{1+\left(\frac{(Cla)_v}{(\pi eAR_v)}\right)^2}+\frac{(Cla)_v}{(\pi eAR_v)}}$ (2) [14]

Setting e=0.95, the coefficients for the horizontal and vertical finite wing of ATLAS I T-tail are presented in Table 2.

ISSN: 2277-9655
Impact Factor: 4.116
CODEN: IJESS7

Table 2: Slopes of ATLAS I T-tail stabilizers lift curves.

T-TAIL AERODYNAMICS - FINITE WINGS		
HORIZONTAL STABILIZER	$(C_{L_a})_h$	0.08169 deg-1
VERTICAL STABILIZER	$(C_{L_a})_v$	0.05608 deg-1

Finally, the contribution of the tail model in flight mechanics will be expressed by the moments it produces in relation to the gravity center of the aircraft. The forces, previously mentioned, multiplied by the distance of the applied point from the gravity center of the aircraft, create the moments of the tail. As before, non-dimensional coefficients will be used for the moments.

The slope of the pitch moment coefficient $(C_{m_a})_t$ of the horizontal tail is given by the equation [6]:

$$(C_{m_a})_t = -(C_{L_a})_h V_h (1 - d\varepsilon/d\alpha) \quad (3)$$

The slope of the yaw moment coefficient $(C_{n_\beta})_t$ of the vertical tail is given by the equation [6]:

$$(C_{n_\beta})_t = (C_{L_a})_v V_v (1 + d\sigma/d\beta) \quad (4)$$

Setting dε/dα = 0 and dσ/dβ = 0 and using the ATLAS I data the slopes of T-tail moment coefficients are presented in Table 3.

Table 3: Slopes of ATLAS I T-tail stabilizers moments.

T-TAIL AERODYNAMICS - MOMENTS		
HORIZONTAL STABILIZER	$(C_{m_a})_t$	$-0.03268\ \text{deg}^{-1}$
VERTICAL STABILIZER	$(C_{n_\beta})_t$	$0.00134\ \text{deg}^{-1}$

The selection of the airfoil comprises one of the most basic steps for the design of an aircraft and it is necessary to be performed after thorough study among many airfoils that have been standardized throughout the years. The airfoil offers appropriate aerodynamic properties to the controlling surfaces of the aircraft. Hence, the aerodynamics engineer has to take into consideration all the parameters so that the airfoil produces the necessary lift and minimum possible drag. The aerodynamic characteristics for the airfoil are:

- Low Reynolds number in the range of 100.000
- Symmetry
- Sufficient lift coefficient C_l
- Low drag coefficient C_d

E472, CG Ultimate, Ultra-Sport, NACA64A010 and SD8020 are airfoils with the appropriate characteristics and they were set under investigation using experimental data. For the comparison of the airfoils a lift to drag ratio graph is used and presented in Figure 2 [12].

ISSN: 2277-9655
Impact Factor: 4.116
CODEN: IJESS7

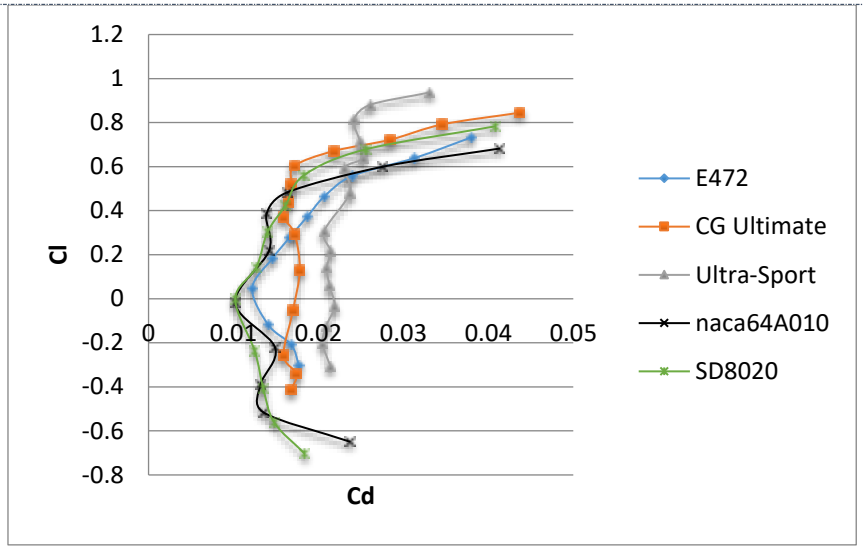

Fig 2: Lift to Drag ratio comparisons for various airfoils at 100.000 Reynolds.

Following the analysis, Ultra-Sport airfoil shows the highest lift coefficient while at the same time it shows the highest drag coefficient for C_l up to + 0.6. The lowest C_d is produced by SD8020 and NACA64A010. Within this area, the selection criterion of low C_d was selected.

The total drag coefficient was investigated using the Lifting Line Theory (LLT) method for finite wings [6]:

$$C_D = C_{d0} + \frac{C_L^2}{\pi ARe} \quad (5)$$

The total drag coefficient relative to angle of attack for the selected airfoils is presented in Figure 3:

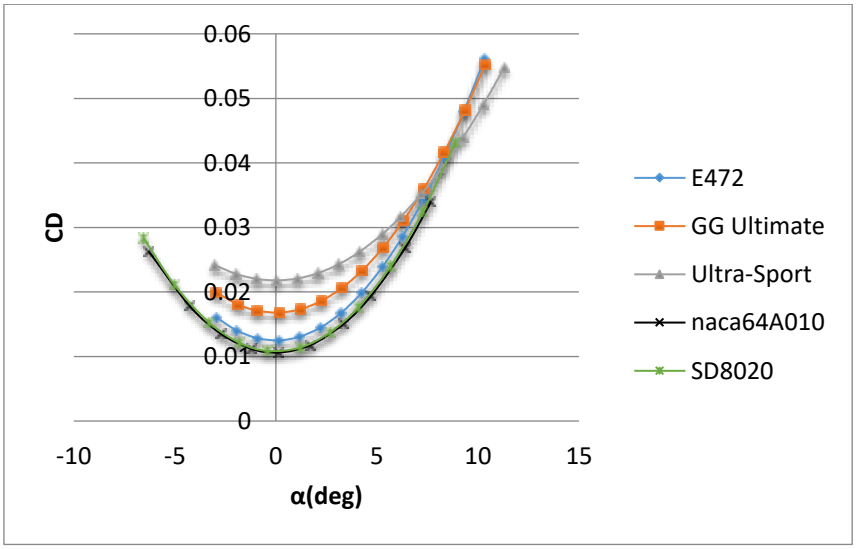

Fig 3: Total Drag coefficient for the selected airfoils in different angles of attack at 100.000 Reynolds.

It was proved that the airfoils SD8020, NACA64A010 and E472 have lower drag coefficient in angle of attacks from -4° to 9°. The final selection is airfoil NACA64A010 because of the low drag coefficient and its aerodynamical characteristics are presented in the Table 4[12].

ISSN: 2277-9655
Impact Factor: 4.116
CODEN: IJESS7

Table 4: Characteristic values of NACA64A010 airfoil.

NACA64A010	
C_{l_a} (deg^{-1})	0.1075
C_{L_a} (deg^{-1})	0.07486
C_{d0}	0.0106
$C_{l_{max}}$	0.81 @ 11°

CONVERSION OF TAIL TYPE "T" TO TYPE "Vee"

The assumptions for the conversion analysis are based on the surface, the stability characteristics and the dihedral angle of the tail [9].

BASIC ASSUMPTIONS

The tail with shape Vee will be considered as a high dihedral angle wing. The load distribution along the wing is based on Line Lift Theory (LLT) for wings without dihedral and swept-back wing and it is assumed to apply on these wings. Moreover, it is assumed that the stability control on the longitudinal and lateral axes is done independently. Also the wing parts of the Vee-tail will be orthogonal.

Studies of NACA [5] for conversion of the conventional tail or T-tail to Vee, showed that the functions for the tail lift coefficient, just as with the side-force coefficient, in relation with the lift coefficient vertically in wing under dihedral angle Γ are the following:

$$C_{L_t} = C_{L_N} \cos \Gamma \quad (6)$$

$$C_{Y_t} = C'_{L_N} \sin \Gamma \quad (7)$$

In addition, as for the stabilizer areas the study on NACA[5] showed that:

$$S_h = S_{vee} \cos^2 \Gamma \quad (8)$$

$$S_v = S_{vee} \sin^2 \Gamma \quad (9)$$

If equation (8) and equation (9) are added by parts we get:

$$S_h + S_v = S_{vee} \left(\cos^2 \Gamma + \sin^2 \Gamma \right) \Rightarrow$$

$$S_h + S_v = S_{vee} \quad (10)$$

DESIGNING STEPS

To estimate the stability derivatives for the Vee-tail the following formulas were used:

$$\left(C_{m_a}\right)_t = -\frac{l_t}{c_w}\frac{S_{vee}}{S_w} C_{L_{a_N}} \cos^2 \Gamma \quad (11)$$

$$\left(C_{n_\beta}\right)_t = \frac{l_t}{b_w}\frac{S_{vee}}{S_w} KC_{L_{a_N}} \sin^2 \Gamma \quad (12)$$

Combining (11) and (12) Vee-tail dihedral is given by:

$$\tan^2 \Gamma = \frac{\frac{b_w}{c_w}\left(C_{n_\beta}\right)_t}{K\left(C_{m_a}\right)_t} \quad (13)$$

The total area of Vee-tail is given by:

$$\frac{S_{vee}}{S_w} = -\frac{\left(C_{m_a}\right)_t}{\frac{l_t}{c_w} C_{L_{a_N}} \cos^2 \Gamma} \quad (14)$$

$$\frac{S_{vee}}{S_w} = \frac{\left(C_{n_\beta}\right)_t}{\frac{l_t}{b_w} KC_{L_{a_N}} \sin^2 \Gamma} \quad (15)$$

ISSN: 2277-9655
Impact Factor: 4.116
CODEN: IJESS7

In order to maintain the same aerodynamic characteristics with the initial T-tail, the coefficients $\left(C_{m_a}\right)_t$ and $\left(C_{n_\beta}\right)_t$ are selected from Table 3.

The process of a Vee-tail design in steps is presented in Figure 4:

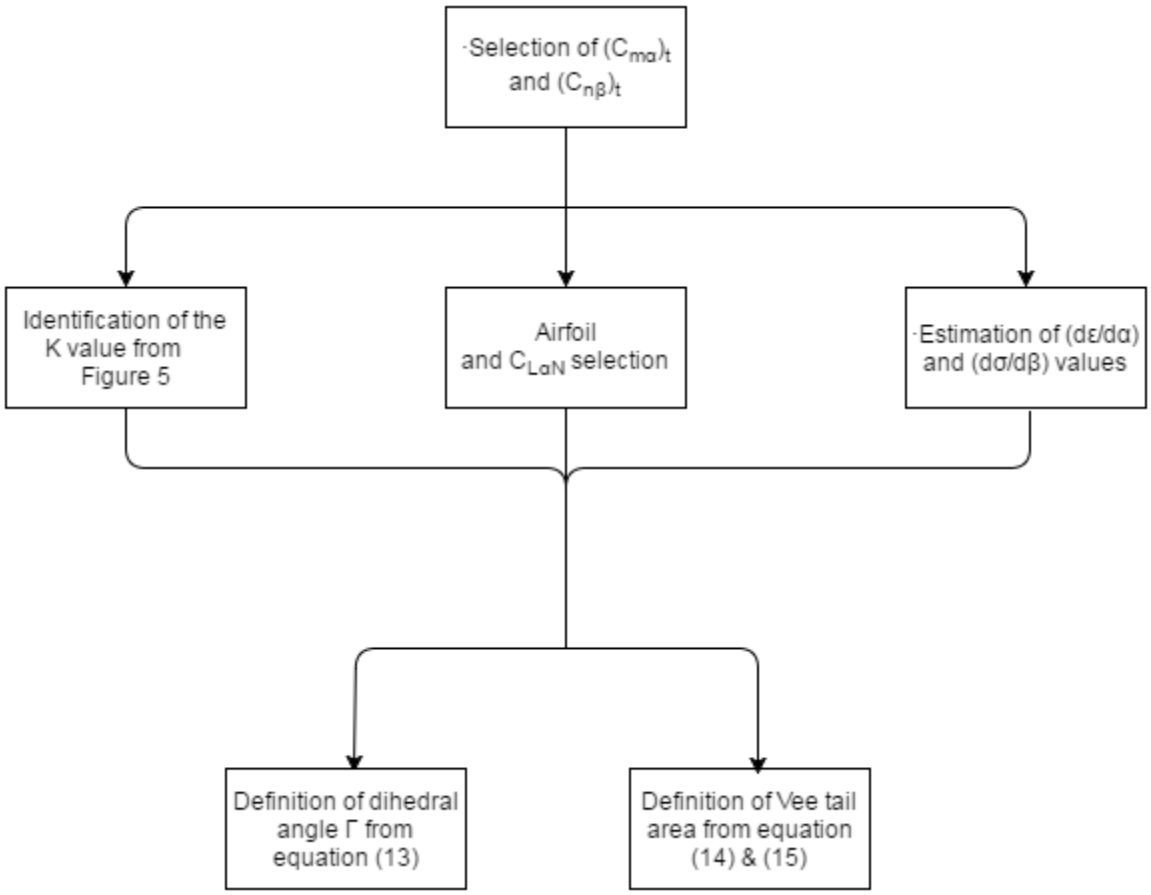

Fig 4: Vee-tail designing steps.

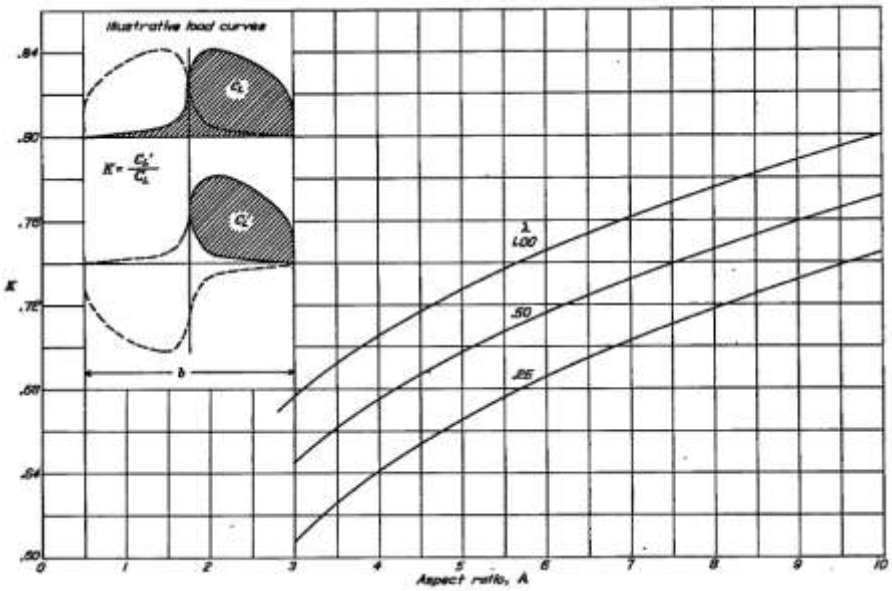

Fig 5: Estimation of K for different AR and λ [5].

ISSN: 2277-9655
Impact Factor: 4.116
CODEN: IJESS7

Setting AR=5 for each wing part of the Vee-tail which is orthogonal, using ATLAS I data and following the design steps, the input and output values of the analysis and the Vee-tail geometry are presented in Table 5. The final total surface of Vee-tail has been rounded upwards for safety.

Table 5: Data and results of the Vee-tail design.

Input Values			Output Values	
$(C_{m_a})_t$ (deg^{-1})	-0.03268		S_{vee} (m2)	0.113
$(C_{n_\beta})_t$ (deg^{-1})	0.001343		Γ (Dihedral Angle)	29°
$C_{L_{a_N}}$ (deg^{-1})	0.07486			
K	0.73		Vee-tail Geometry	
S_w (m2)	0.45504		S_{vee} (m2)	0.12
l_t (m)	0.662		b (m)	0.77
c_w (m)	0.288		c (m)	0.157
b_w (m)	1.58		AR	5
dε/dα	0		Λ	0°
dσ/dβ	0		λ	1

Fig 6: Vee-tail design

COMPUTATIONAL 2-D STUDY OF NACA64A010 AIRFOIL

The 2-D computational study of airfoil NACA64A010 was carried out using ANSYS Fluent. The scope of the computational analysis is to confirm the experimental and theoretical results regarding the aerodynamic coefficients as well as to calculate the boundary layer of the flow around the airflow in order to be used for analyzing the three-dimensional tail.

The steps that followed for the computational analysis were:

- Airfoil Geometry and Boundary Conditions identification
- Grid construction around NACA64A010
- Air's physical parameters definition
- Turbulence model and Numerical method selection
- Results post processing

In current study, for the surrounding environment, type C is used and its limits is far enough away from the airfoil. In particular, the semicircle has a radius of 12 times the chord of the airfoil (c=1m) and the rectangle has a length of 20 times the chord of the airfoil. Thus the semicircle has a radius of 12 m and the rectangle has a length of 20m and a width which is determined by the semicircle 24m. Also, the boundary conditions of the analysis are presented in Figure 7.

ISSN: 2277-9655
Impact Factor: 4.116
CODEN: IJESS7

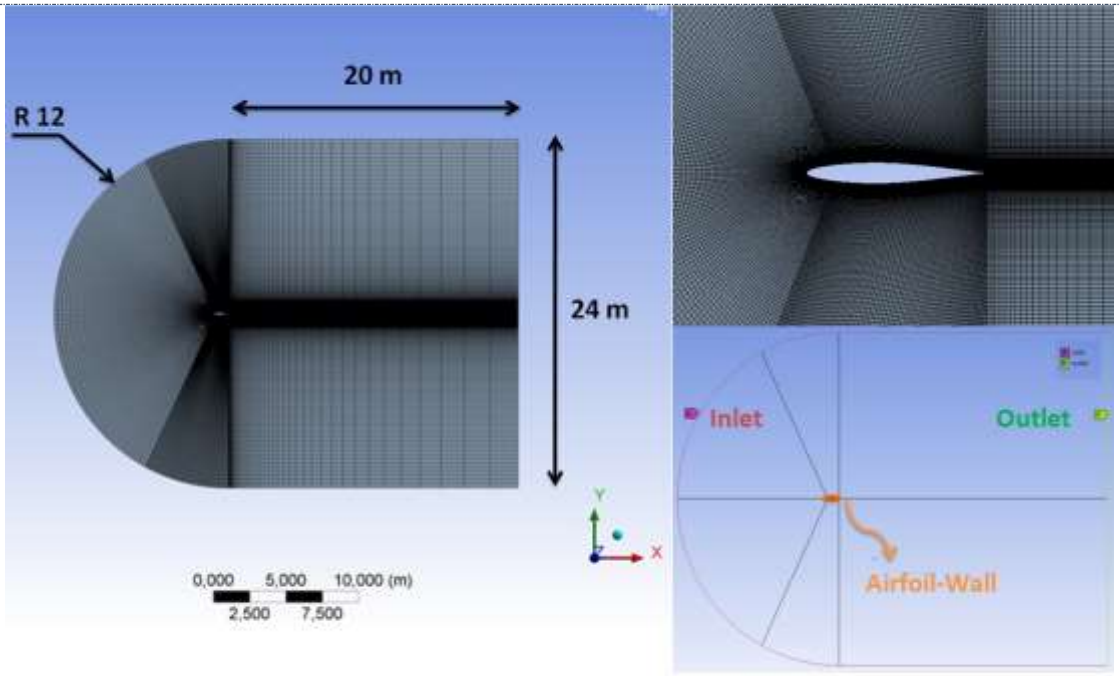

Fig 7: Computational grid and boundary conditions of the 2-D airfoil analysis

The boundary conditions parameters are presented in Table 6.

Table 6: Boundary conditions for 2-D airfoil analysis.

Boundary	Boundary condition
Inlet	Velocity inlet - U = 1.82 m/s
Outlet	Pressure Outlet Gauge Pressure = 0 Pa
Airfoil	Wall

The grid size was selected after a study of its convergence was performed. Having as criteria the lift and drag coefficients, flow analysis of different grid sizes was carried out. The scope of the independency of the grid is for the rates of the critical aerodynamic parameters (C_l and C_d) to remain stable as the number of nodes increase and the grid becomes larger. Then the results of the analysis are reliable and the smallest possible grid can be selected which will give the same results as the next larger ones.
The grid has the following characteristics:

Table 7: Computational grid parameters for 2-D airfoil analysis.

Elements	Nodes	Skewness	Orthogonal Quality
80.000	80.550	0.09	0.978

In Table 8 the physical properties for the air domain are summoned.

Table 8: Air physical properties for the 2-D airfoil analysis.

Input Values	
Air Pressure - P (Pa)	101325
Air Velocity - U (m/s)	1.82
Air Density - ρ (Kg/m^3)	1.225
Air Dynamic Viscocity μ (Pa·s)	1.7894×10^{-5}
Air Temperature - T (K)	288.16

ISSN: 2277-9655
Impact Factor: 4.116
CODEN: IJESS7

Reference Area A_{ref} (m^2)	1
Turbulence Intensity - I	0.5%
Turbulence Length l_{turb} (m)	0.024

The discretization of the Navier-Stokes equations that Fluent uses is carried out with the method of the finite volumes. The computational analysis parameters are presented in Table 9.

Table 9: Computational analysis parameters.

Analysis Parameters	
Solver Setup	Density-Based
Time	Steady State
Turbulence models	Spalart-Allmaras SST k-ω Realizable k-ε
Solution Scheme	Implicit

XFLR5 is a software for the design and analysis of subsonic airfoils and wings and it was used for an analysis based on the LLT method with neglected viscosity (Euler Flow). The results that derive from the computational analysis are compared with experimental and XFLR5 results and are presented in Figure 8 and Figure 9.

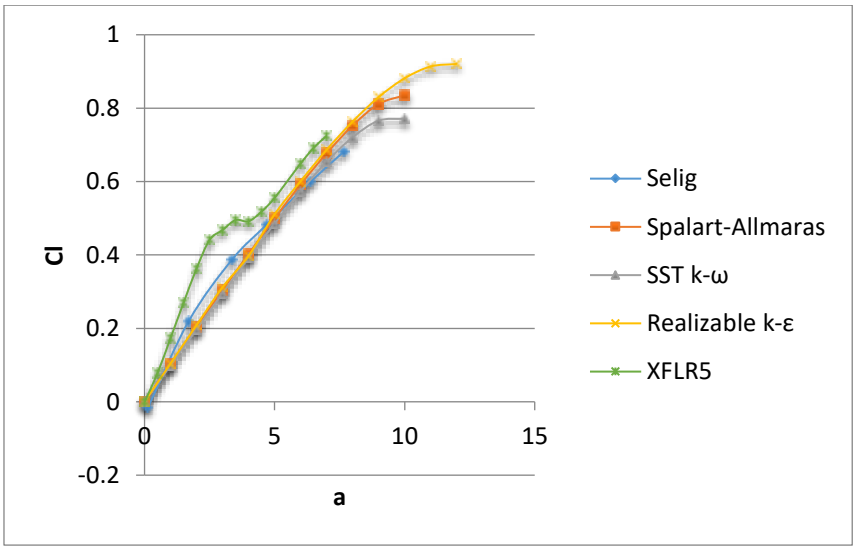

Fig 8: NACA64A010 C_l curves comparisons for different turbulence models and experimental data at 128.976 Re.

Following Figure 8 it seems that all the turbulence models follow Selig's experimental values but not the values from the XFLR5. The XFLR5 analysis shows a deviation in the 2° – 3° angle of attack region. The three turbulence models coincide at small angles of attack and start to deviate after the 8° angle showing possible flow destabilization and separation. Following the literature the SST k-ω model is the most conservative and gives smaller values to the lift coefficient while the Realizable k-ε model gives the highest C_l values and continues until the 12°. The Spalart-Allmaras model seems to give intermediate values relative to the previous ones.

ISSN: 2277-9655
Impact Factor: 4.116
CODEN: IJESS7

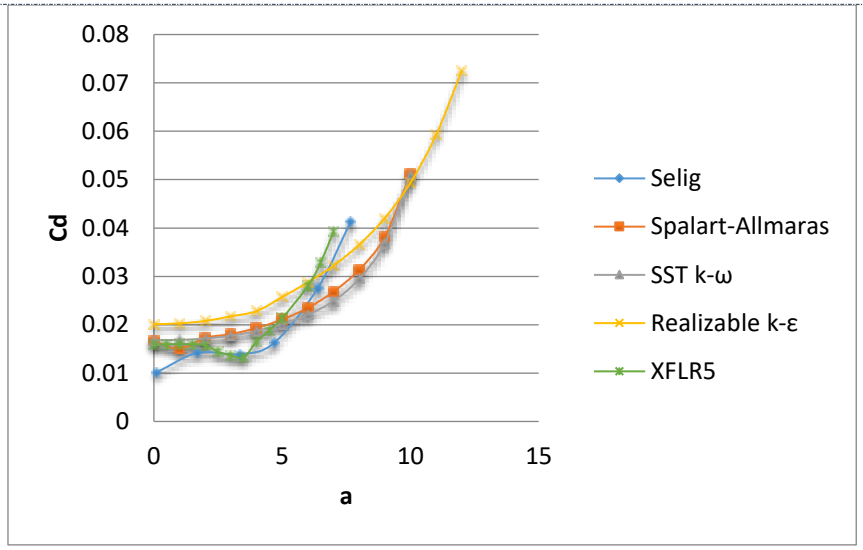

Fig 9: NACA64A010 C_d curves comparisons for different turbulence models and experimental data at 128.976 Re.

Figure 9 shows that only the result of the XFLR5 follows the abrupt variations of the experimental drag coefficient while the results of the fluent follow a more smooth variation. Again the SST k-ω model is the most conservative and almost coincides with that of the Spalart-Allmaras while the Realizable k-ε model gives the highest C_d values.

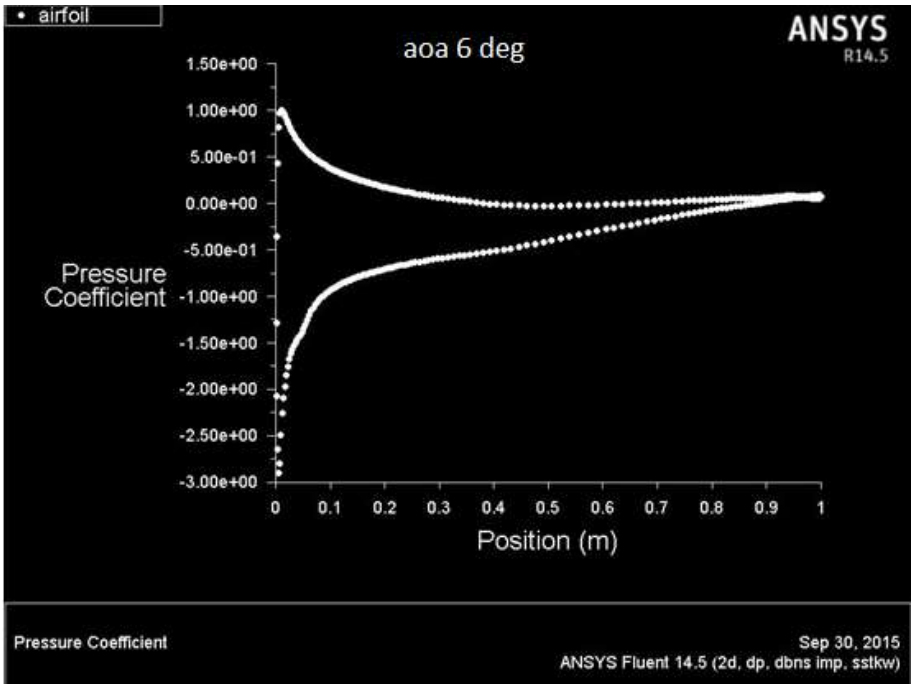

Fig 10: NACA64A010 Pressure Coefficient with SST k-ω model at 6°angle of attack at 128.976 Re.

ISSN: 2277-9655
Impact Factor: 4.116
CODEN: IJESS7

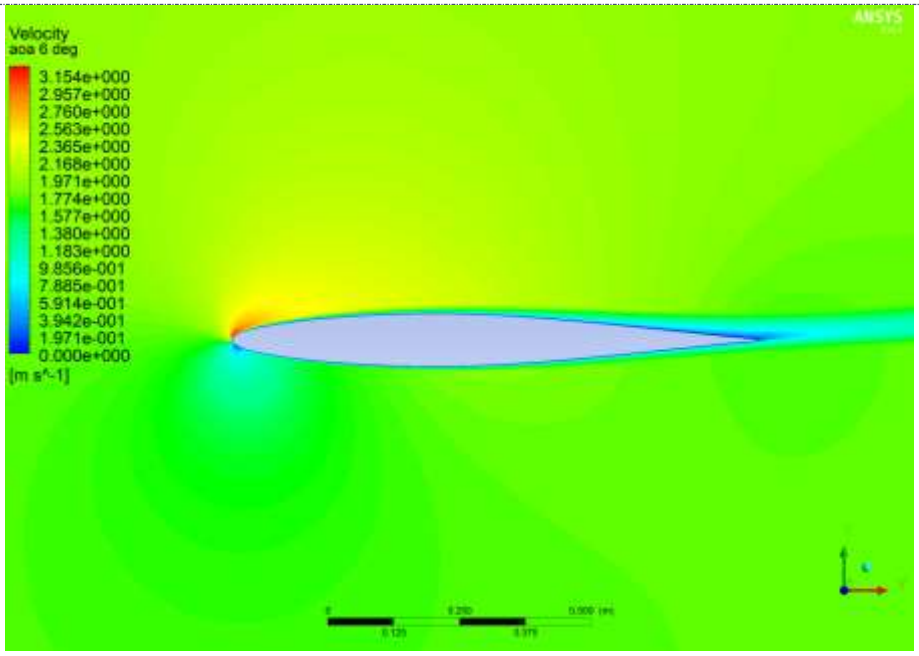

Fig 11: NACA64A010 Velocity Contours with SST k-ω model at 6°angle of attack at 128.976 Re.

COMPUTATIONAL 3-D STUDY OF THE Vee-TAIL

The analysis continues from the 2-D airfoil to the 3-D Vee-tail. In a 3-D analysis the computational grid is consisted of a large amount of nodes, and a huge computing memory is necessary in order to perform the analysis. Also the Vee-tail geometry is complex and a selection of the appropriate grid is difficult. For these reasons, an unstructured grid was selected because of its smaller number of nodes relative to a structured grid. The region near the Vee-tail is critical because of the phenomena that take place in and near the boundary layer. In order to notice these phenomena, the grid has to be dense and structured in this region so it is important to perform a boundary layer analysis.

The boundary layer is estimated performing a 2-D analysis for an airfoil chord c = 0.157m and Reynolds 128.976 resulting that the width of the boundary layer is δ_{99} = 0.006m as shown in Figure 12.

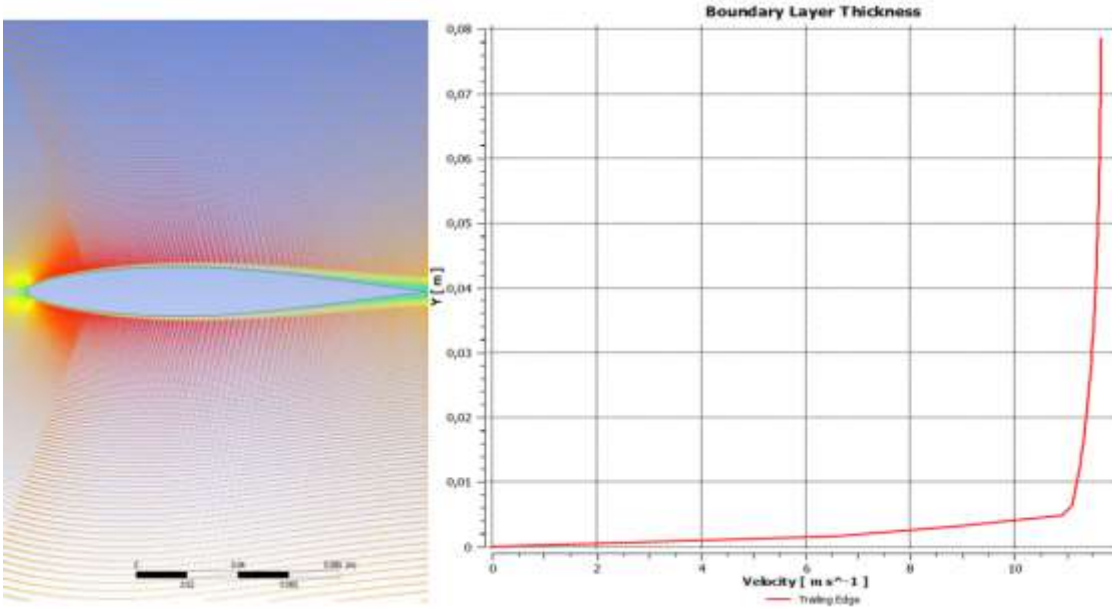

Fig 12: NACA64A010 boundary layer at 128.976 Reynolds.

ISSN: 2277-9655
Impact Factor: 4.116
CODEN: IJESS7

The 3-D computational analysis was performed for the Vee-tail for different angles of attack (around y-axis) and side-slip (around the z-axis) in order to study its aerodynamical performance during flight. These two angles are explained in Figure 13.

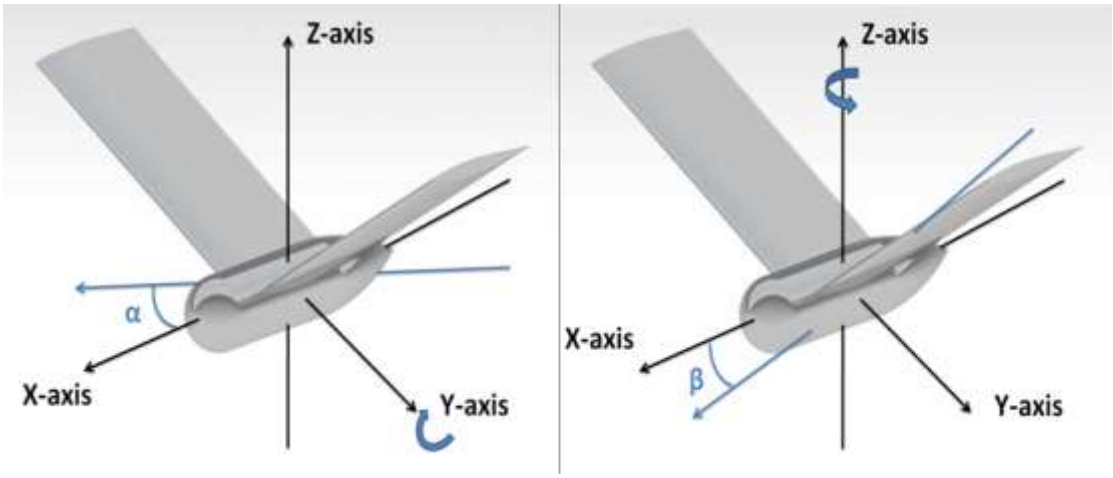

Fig 13: Left: Vee-tail angle of attack. Right: Vee-tail angle of sideslip.

The geometry design of the Vee-tail will also include a Rankine body which assists to normalize the flow aerodynamically. The next step is to construct the domain which is consisted of two side planes below, 2m long, with an angle equal to the angle of the dihedral of 29 degrees and a curvilinear surface of a 2m radius on the top. The tail within the area has a distance from the inlet equal to 5 times the chord and from the outlet equal to 10 times the chord.

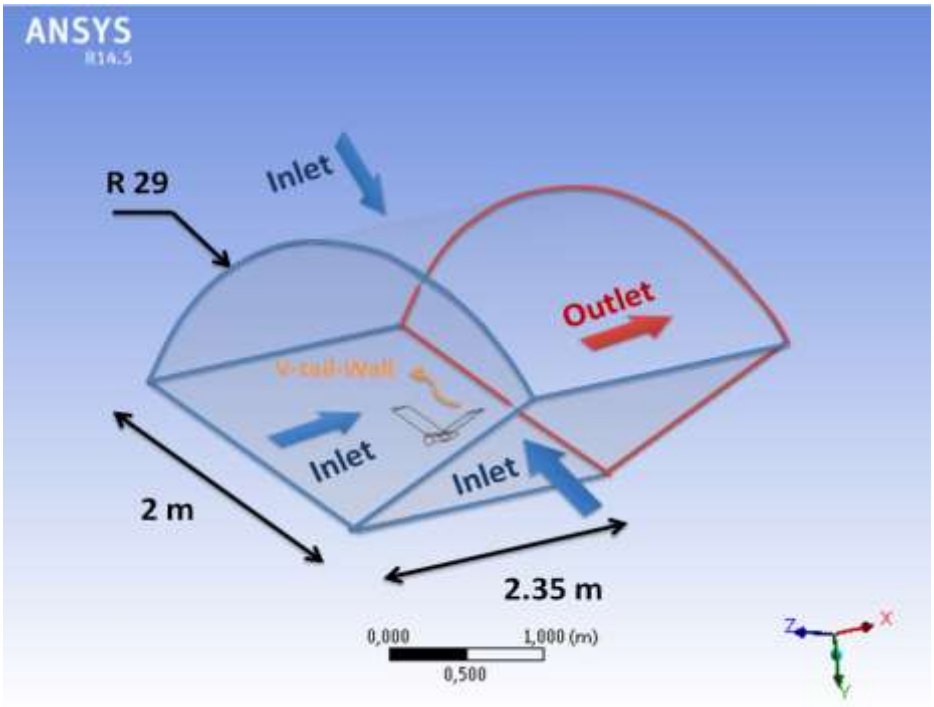

Fig 14: Computational grid and boundary conditions of the 3-D Vee-tail analysis.

The boundary conditions parameters are presented in Table 10:

ISSN: 2277-9655
Impact Factor: 4.116
CODEN: IJESS7

Table 10: Boundary conditions for 3-D Vee-tail analysis.

Boundary	Boundary condition
Inlet	Velocity inlet - Ux = 12 m/s
Outlet	Pressure Outlet - Gauge Pressure= 0 Pa
Vee-tail	Wall

The computational grid near the Vee-tail is structured in order to notice the flow in the boundary layer level. The inflation method was used and the parameters are presented in Table 11.

Table 11: Inflation parameters.

Inflation Parameters	
y^+	1
First Layer Thickness	2.8e-05m
Number of Layers	32
Growth Rate	1.2

The computational grid, besides the inflation, is unstructured because of the complex geometry of the tail. Images of the grid on intersections of the surrounding environment with the tail are presented in Figure15, Figure 16 and Figure 17.

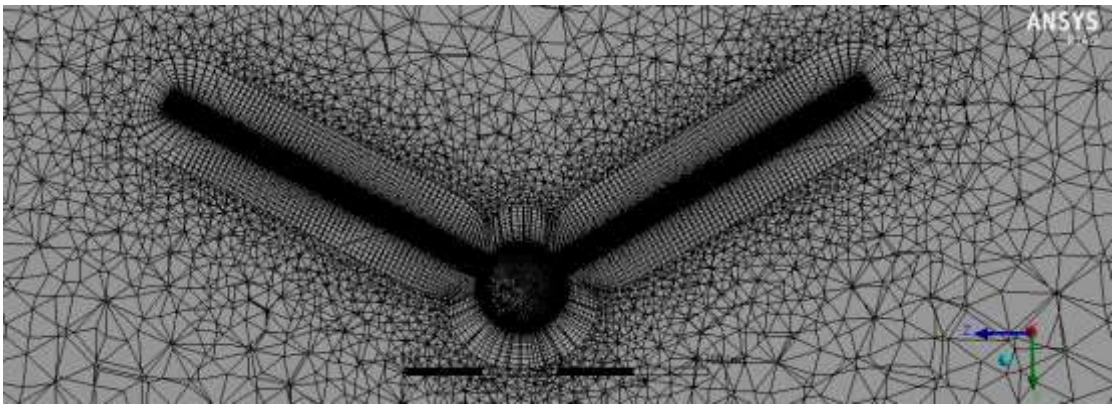

Fig 15: Intersection of the domain.

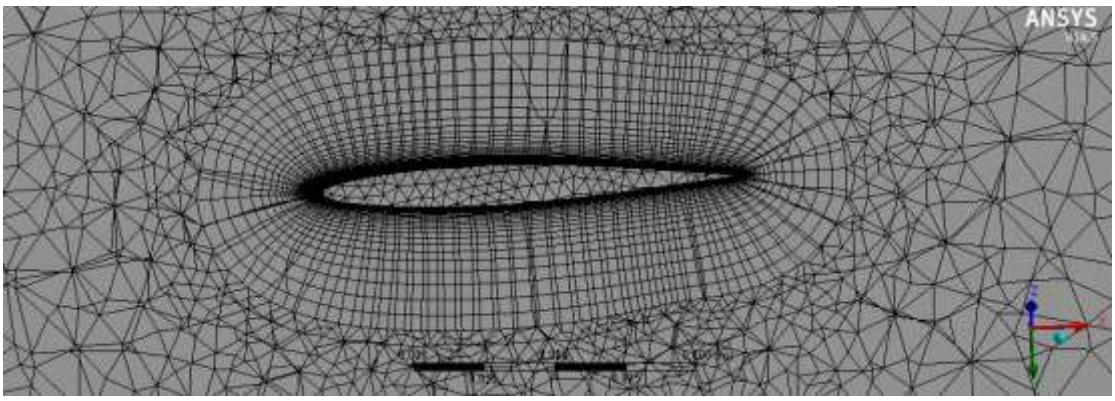

Fig 16: Intersection of the domain with the wing.

ISSN: 2277-9655
Impact Factor: 4.116
CODEN: IJESS7

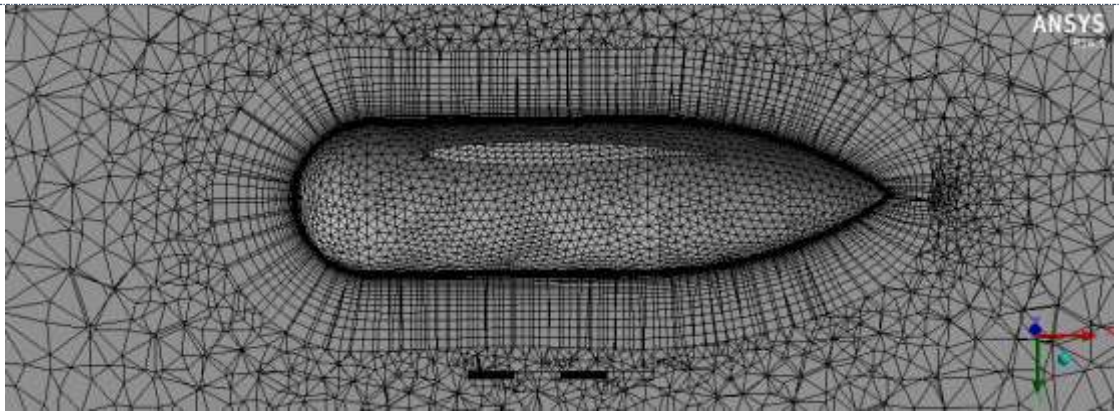

Fig 17: Intersection of the domain with the Rankine body.

The grid has the following characteristics:

Table 12: Computational grid parameters for 2-D airfoil analysis.

Elements	Nodes	Skewness	Orthogonal Quality
1281158	504922	0,33	0,8

The physical properties for the air domain are summoned in Table 13.

Table 13: Air physical properties for the 3-D Vee-tail analysis.

Input Values	
Air Pressure - P (Pa)	101325
Air Velocity - U (m/s)	12
Air Density - ρ (Kg/m^3)	1,225
Air Dynamic Viscocity μ (Pa·s)	1.7894×10^{-5}
Air Temperature - T (K)	288,16
Reference Area A_{ref} (m^2)	0,12
Turbulence Intensity - I	0,5%
Turbulence Length l_{turb} (m)	0,024

The computational analysis parameters are presented in Table 14.

Table 14: Computational analysis parameters.

Analysis Parameters	
Solver Setup	Pressure-Based
Time	Steady State
Turbulence models	Spalart-Allmaras SST k-ω Realizable k-ε
Solution Scheme	SIMPLE

ANALYSIS OF ANGLES OF ATTACK RESULTS

An approach for the aerodynamic coefficients of the tail complex was made with the use of the analytical relations of the Lifting Line Theory (LLT) as well as in combination with pilot results from the wind tunnel that SELIG performed for the UIUC Low-Speed Airfoil program me. In particular these results had to be combined with the formulae

$$C_{L_t} = C_{L_N} \cos \Gamma \quad (16)$$

ISSN: 2277-9655
Impact Factor: 4.116
CODEN: IJESS7

so that the dihedral will be taken into account and that the aerodynamic coefficients be converted to a vertical layer with the wings.

The computational results obtained from the three different turbulence models and analytical methods are presented in Figure 18, Figure 19 and Figure 20.

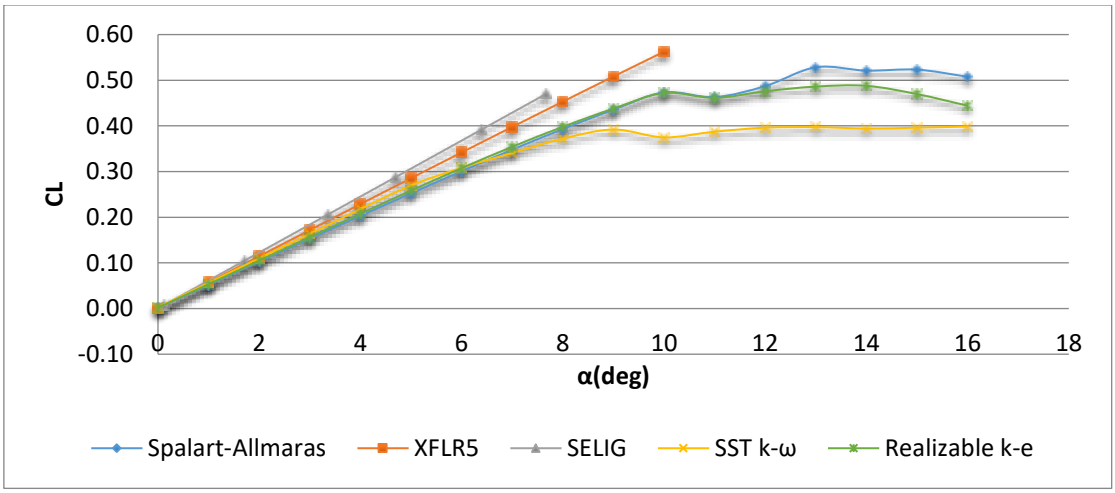

Fig 18: Vee-tail lift coefficient vs angle of attack for various turbulence models and analytical methods at 128.976 Re.

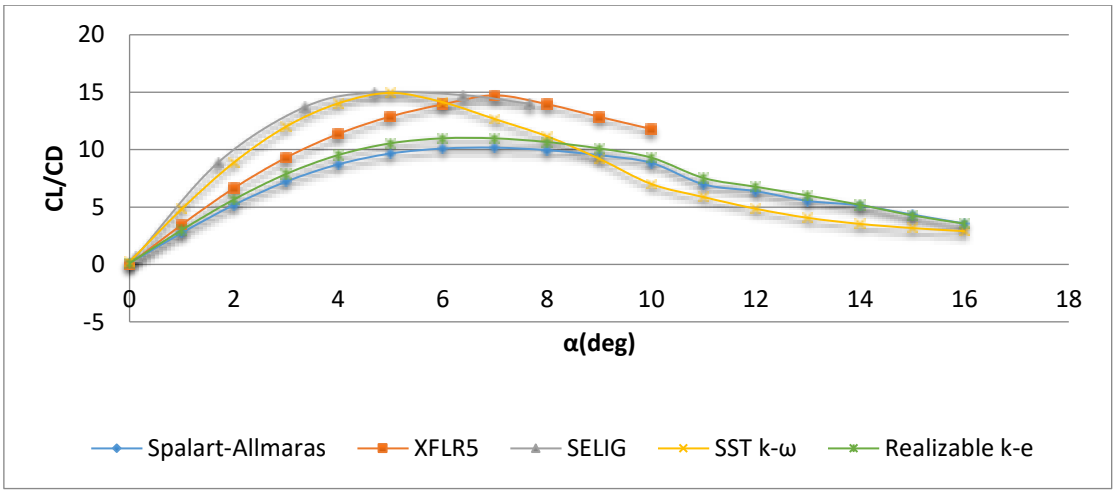

Fig 19: Lift to Drag ratio comparisons for various turbulence models and analytical methods at 128.976 Re.

ISSN: 2277-9655
Impact Factor: 4.116
CODEN: IJESS7

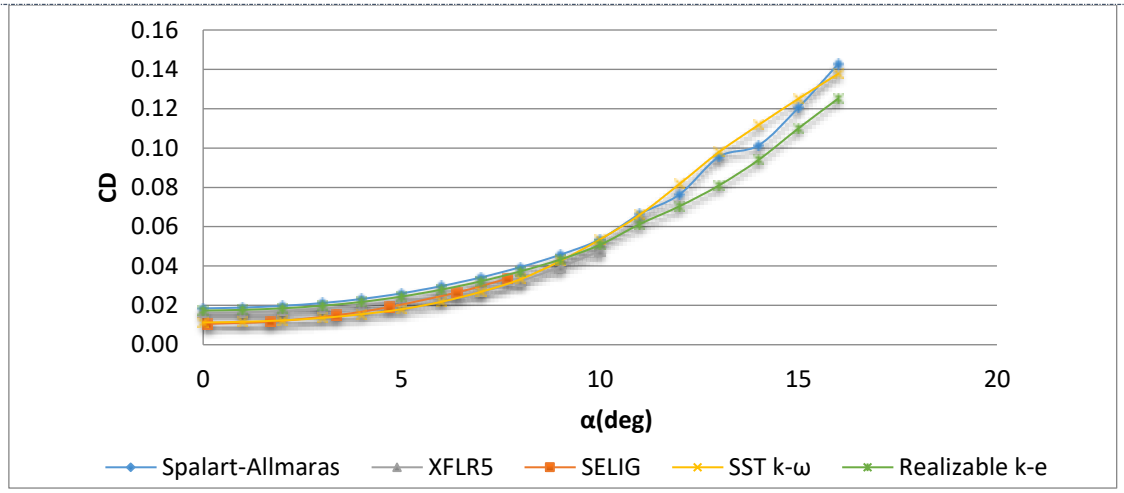

Fig 20: Vee-tail drag coefficient vs angle of attack for various turbulence models and analytical methods at 128.976 Re.

It must be noted that all of the results agree with the linear area, while beyond this, the XFLR5 and the analytical relations continue accordingly while the computational analysis take into account the separations and are differentiated.

The Vee-tail loses its aerodynamic efficiency at high angles of attack (> 10 degrees) because of the flow separation. The streamlines around the tail are presented in Figure 21.

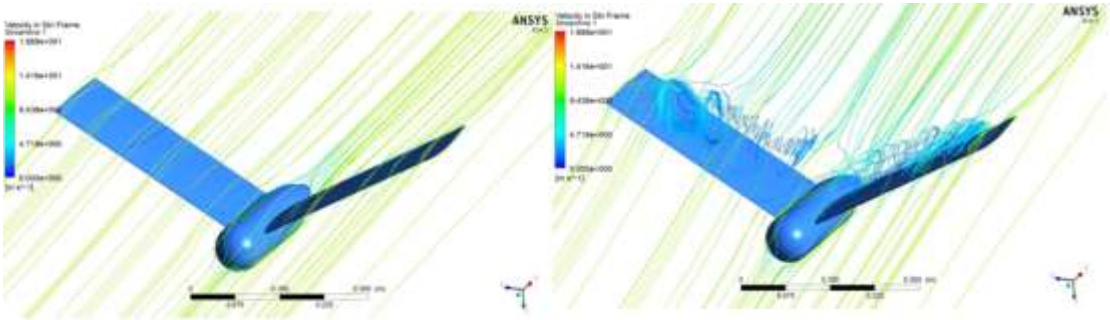

Fig 21: Left: Streamlines at 6° angle of attack. Right: Streamlines at 16° angle of attack at 128.976 Re.

ANALYSIS OF ANGLES OF SIDESLIP RESULTS

The analysis for the slide-slip angles have been defined with a constant (trim condition) angle of attack at 6° that is necessary for the horizontal flight of ATLAS I. In particular, the horizontal stabilizer of ATLAS I has been adjusted to an angle of incidence -5° with NACA 0012, which is translated to C_L = 0.3. The Vee-tail after the above mentioned analysis of the angles of attack shows C_L = 0.3 at 6°. Thus, in this way the fixed angle of attack which all the slide-slip analysis will have was defined. The results of the analysis which were produced are shown below.

ISSN: 2277-9655
Impact Factor: 4.116
CODEN: IJESS7

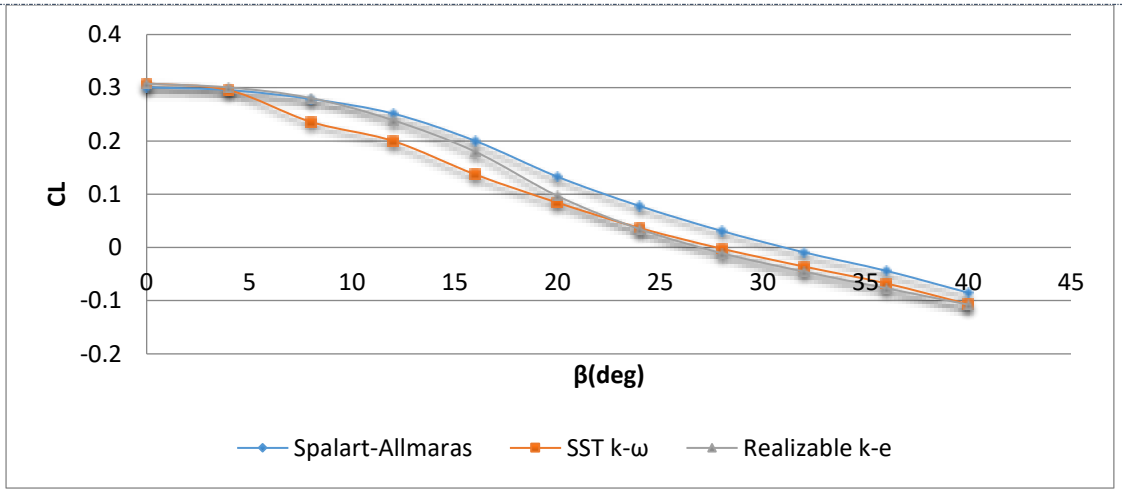

Fig 22: Vee-tail lift coefficient vs angle of sideslip for various turbulence models at 128.976 Re.

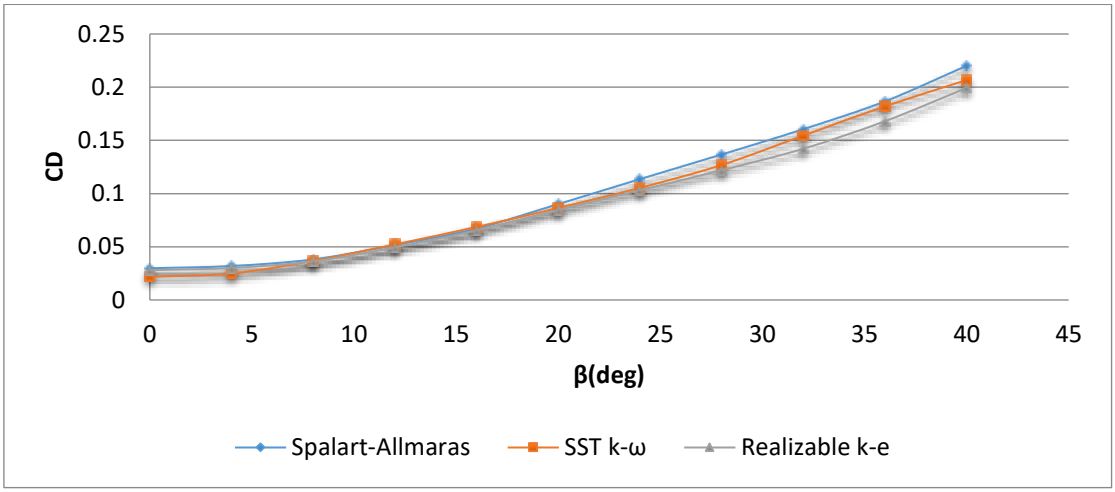

Fig 23: Vee-tail drag coefficient vs angle of sideslip for various turbulence models at 128.976 Re.

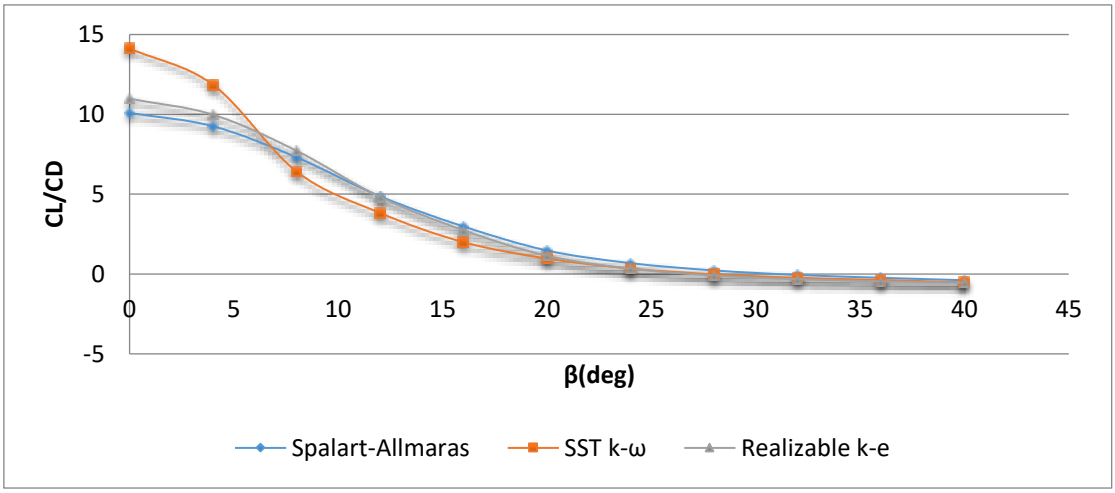

Fig 24: Lift to Drag ratio comparisons for various turbulence models at 128.976 Re.

It must be noted that all of the results from all the turbulence models are in agreement. Also, the Vee-tail lose its aerodynamical efficiency at high angles of sideslip (> 7 degrees) because of the flow separation phenomenon. The streamlines around the tail are presented in Figure 25.

ISSN: 2277-9655
Impact Factor: 4.116
CODEN: IJESS7

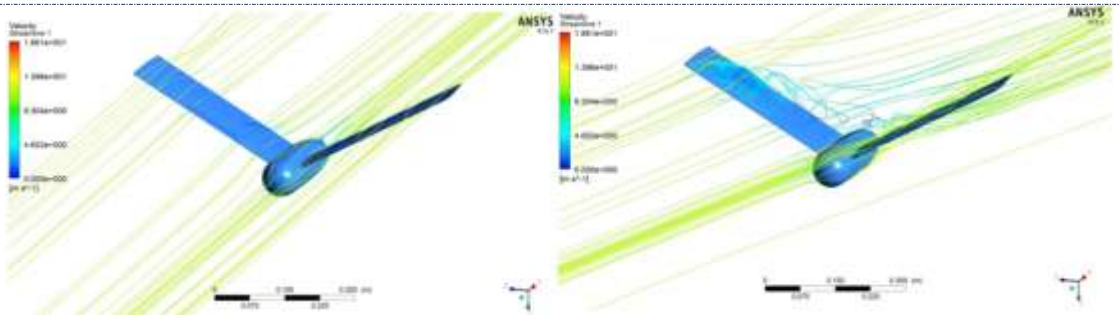

Fig 25: Left: Streamlines at 4° angle of sideslip. Right: Streamlines at 24° angle of sideslip at 128.976 Re.

CONCLUSION

In conclusion, the results showed that the theoretical solutions are in agreement with the computational calculations and the computational procedure is confirmed. For the Vee-tail arose that the C_L follows a linear variation in relation with the angle of attack till the 7°. Later the solution with the turbulence models starts to diverge, with the SST k-ω giving the most preservative results. For the C_D in relation to the angle of attack observed a convergence between the different turbulence models but also between the theoretical results.
With the increase of the slide-slip angle observed loss of the aerodynamic performance of the tail complex. Till the 8° a 30% increase of the C_D is observed and a 9% C_L reduction. At 12° the raise of the C_D is at 76% and at 24° the aerodynamic performance goes to zero.

ACKNOWLEDGEMENTS

The authors wish to acknowledge all their teammates of UPat ATLAS Team and co-members of ATLAS Aero Group for their efforts (2006-now) to design, build and fly innovative radio-controlled/autonomous unmanned aircrafts investigating cross-edge aerodynamic and flight stability phenomena.

REFERENCES

[1] Barnes W. McCormick, Second Edition, (1995) Aerodynamics, Aeronautics, and Flight Mechanics, Wiley Aeronautics and Aerospace.
[2] Roskam, J. (2005) Airplane Design, vol. I, DAR Corporation Anderson, J.D. (1999) Aircraft Performance and Design, McGraw-Hill.
[3] Robert C. Nelson Second Edition, FLIGHT STABILITY AND AUTOMATIC CONTROL, McGraw-Hill.
[4] Eckalbar, John C. (1986), Simple Aerodynamics of the V-Tail.
[5] Purser, Paul E.; and Campbell, John P. (1945) : Experimental Verification of a Simplified Vee-Tail Theory and Analysis of Available Data on Complete Models With Vee Tails. NACA Rep. 823. (Supersedes NACA ACR L5A03.)
[6] Mark Drela, (2014), "Flight Vehicle Aerodynamics", MIT Press.
[7] ATLAS Aero Team, (2007), "ATLAS I Report", University of Patras.
[8] Pass H.R. (1940): Analysis of Wind - Tunnel Data on Directional Stability and Control. NACA TN No. 775.
[9] Mohammad H, Sadraey, (2013), AIRCRAFT DESIGN A System Engineering Approach, Wiley Aeronautics and Aerospace.
[10] Daniel P. Raymer, Second Edition, (2004), Aircraft Design: A Conceptual Approach, AIAA Education Series.
[11] Roskam J., Edward Lan Chuan-Tau, (1997), Airplane Aerodynamics and Performance, DAR Corporation.
[12] Selig S. M. , Gulielmo J. J. , Broeren P. A. , Giguere P. , (1995), Summary of Low-Speed Airfoil Data V1, SoarTech Publications.
[13] Anderson, John D. (2001), Fundamental of aerodynamics, McGraw-Hill, Boston.
[14] D.Küchemann. (1956), A Simple Method for Calculating the Span and Chordwise Loading on Straight and Swept Wings of any Given Aspect Ratio at Subsonic Speeds. R. & M. No. 2935 (15,633) A. R. C. Technical Report.